

# Polymer-Based Open-Channel Blockers for the Acetylcholine Receptor: The Effect of Spacer Length on Blockade Kinetics<sup>†</sup>

Wan-Chen Lin and Stuart Licht\*

Department of Chemistry, Massachusetts Institute of Technology, 77 Massachusetts Avenue, Cambridge, Massachusetts 02139

Received April 25, 2008; Revised Manuscript Received June 17, 2008

**ABSTRACT:** Blocking open ion channels provides a promising way to modulate synaptic transmission. Using the muscle-type acetylcholine receptor (AChR) as a test system, we seek to develop blockers that have blockade kinetics tunable via structural modifications. Here we investigate whether the blockade kinetics can be modulated by specifying the length of a poly(ethylene glycol) (PEG) spacer incorporated into the blocker. Single-channel electrophysiological experiments show that simple bis(trimethylammonium) compounds (**1a–3**) both activate the AChR and block the open channel. The blockade kinetics are found to depend on spacer length: both the association and dissociation rate constants decrease with increasing spacer length. The decrease in the association rate constant can be quantitatively explained by the entropic cost of polymer confinement in the transmembrane lumen, while the decrease in the dissociation rate constant is consistent with weak, additive noncovalent interactions between the channel and the spacer. These results provide useful insights into the future design of kinetically tunable open-channel blockers for the AChR.

Ion channels are essential mediators of signaling in the nervous system. Because of their importance in neuronal communication and other cellular signaling pathways, ion channels are a major class of drug targets (1–4). Ion channels mediate communication between presynaptic and postsynaptic cells at synapses. The kinetics of synaptic signaling are modulated by the gating kinetics of ion channels, that is, the rates of channel opening and closing. The opening of an ion channel allows ions to permeate the cell membrane, resulting in changes in the transmembrane electric potential. At synapses, information processing can be governed by the properties of electric signals that propagate through the cell membrane, with narrower waveforms allowing better temporal precision of transmission (5, 6). Alterations in the kinetics of current flow through ion channels may therefore cause profound effects on synaptic transmission.

Because of the link between ion channel kinetics and the properties of synaptic signals, channel inhibition can be used to modulate synaptic transmission. Some channel inhibitors block ionic currents by occupying the open pore (the central pathway formed by the transmembrane domains) of the activated channel. These inhibitors allow channels to open but transiently prevent ion flow via association of the blocker with the open pore. Inhibitors of this type (open-channel blockers) can either accelerate or prolong the decay of synaptic currents. When blockade is short-lived but the blocker-occupied channel cannot return to the resting closed conformation, the brief blockade events convert each opening event into a prolonged burst of short openings and brief blockades (7), thereby prolonging the macroscopic current

decay (8). When blockade is long-lived, the blockade events terminate channel openings, accelerating the decay of synaptic currents (9, 10).

Due to the wide range of blockade kinetics provided by small molecules, open-channel blockade is a promising method for tuning the kinetics of synaptic transmission. For instance, quinidine has been used clinically for treatment of “slow channel” congenital myasthenic syndromes by causing long-lived open-channel blockade of the nicotinic acetylcholine receptor (AChR),<sup>1</sup> which accelerates the decay of postsynaptic currents (11). Although a variety of small molecules have been characterized to target open channels, rational design of open-channel blockers has been challenging, mainly due to the paucity of high-resolution structures for ion channels. Nonetheless, prediction of blockade kinetics within a series of compounds can be feasible. Previous work on a series of piperazinium (PIP) derivatives has shown that the blocker dissociation rate constant varies systematically with the length of the alkyl tail and that the contribution of each methylene unit to the activation free energy for dissociation is additive (12). When the length of the alkyl tail is extended from one to six carbons, the dissociation rate of the blocker decreases from  $1.4 \times 10^5 \text{ s}^{-1}$  to  $9.8 \times 10^2 \text{ s}^{-1}$ , leading to a ~80-fold enhancement in the blockade affinity. The observation indicates that the dissociation rate and/or affinity of an open-channel blocker can be systematically modulated if the interactions between the binding element and the transmembrane pore are additive. For applications in modulating synaptic currents, it is desirable

<sup>†</sup> This work was supported by the Beckman Foundation (to S.L.) and a Merck-MIT Graduate Fellowship (to W.L.).

\* To whom correspondence should be addressed. Telephone: (617) 452-3525. Fax: (617) 258-7847. E-mail: lights@mit.edu.

<sup>1</sup> Abbreviations: ACh, acetylcholine; AChR, acetylcholine receptor; CCh, carbamylcholine; PEG, poly(ethylene glycol); PPTMA, phenylpropyltrimethylammonium; PIP, piperazinium; QA, quaternary ammonium; TMA, tetramethylammonium; TEA, tetraethylammonium; SKM, segmented k-means; MIL, maximum interval likelihood.

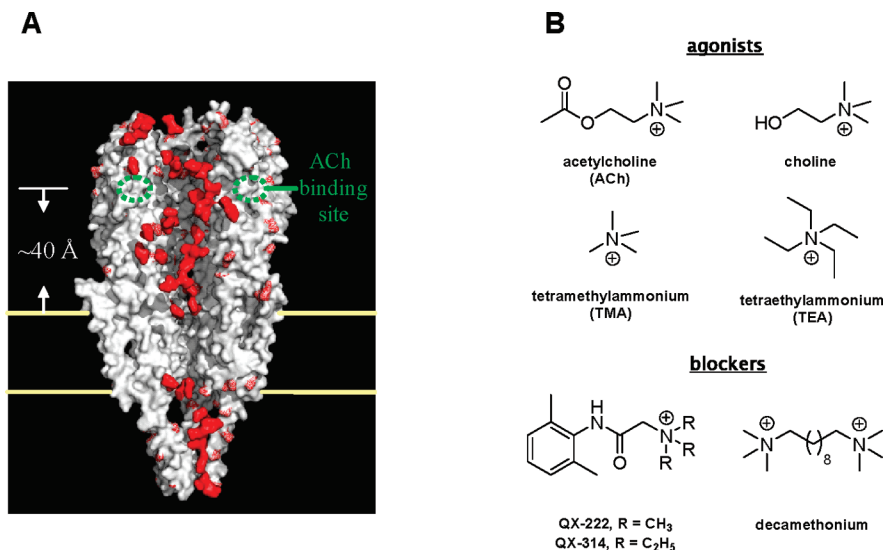


FIGURE 1: (A) The structure of *Torpedo* AChR (surface map; PDB entry 2BG9) (18). Only three subunits (from left to right:  $\delta$ ,  $\alpha$ ,  $\gamma$ ) are plotted in order to show the inner surface of the vestibule chambers. The transmembrane portion of the receptor is indicated by the yellow lines, the location of agonist binding sites is indicated by green dashed circles, and the negatively charged residues (Glu and Asp) are highlighted in red. (B) Examples of quaternary ammonium-based agonists and blockers for the AChR. The agonists presented here also function as open-channel blockers at millimolar concentrations.

to have blockers that span a broad range of dissociation rate constants, since this would allow access to a broad range of synaptic current kinetics.

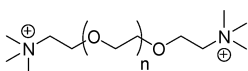
Compared to the alkyl chains incorporated in PIP derivatives, polymer scaffolds might have the advantage of expanding the range of kinetic modulation, since their broader size range may translate to a broader energetic range of channel-blocker interactions. Most open-channel blockers identified to date are small molecules or peptides; polymers have not yet been reported as a scaffold for channel blockers. However, free or covalently attached polymers have been reported to partition efficiently into the transmembrane lumen of a bacterial ion channel, reducing the channel's mean conductance (13, 14). These observations inspired us to use structurally flexible polymers as a scaffold for open-channel blockers. Unlike the docking mode of binding expected for rigid small-molecule blockers, flexible polymers are expected to adopt conformations that maximize favorable interactions with the channel pore. According to the study of PIP derivatives, binding affinity can be modulated by the extent of nonpolar interactions between the blocker and the pore region (12). The weak hydrophobic or van der Waals interactions between the channel and each monomer unit are expected to be additive, allowing the control of the blocker's dissociation rate. In addition, the association rate constant of a polymer-based blocker is also predicted to depend on the size of the polymer backbone, due to the entropic cost associated with the entry of a polymer into the channel pore (15). Systematic modification of the polymer length is therefore likely to provide predictable blockade kinetics of the resulting blockers.

The mammalian muscle-type AChR provides a useful test system for evaluating the proposed design strategy, since a wealth of kinetic and structural information is available for this channel. The AChR is a pentameric transmembrane protein (assembled as a ring of  $\alpha$ ,  $\epsilon$ ,  $\alpha$ ,  $\beta$ , and  $\delta$  subunits in the adult isoform) present in the postsynaptic membrane of the neuromuscular junction (16, 17). Upon binding two molecules of agonist (e.g., acetylcholine), the channel

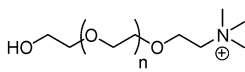
undergoes conformational changes in a "gate" region embedded in the cell membrane, opening its central pore and allowing small cations to pass. The structure of the intact channel (refined to 4 Å resolution) has provided a detailed molecular view of the essential structural components (18). The extracellular vestibule (i.e., the central chamber defined by the extracellular domains of the subunits) is lined with negatively charged residues that may provide electrostatic interactions with passing cations; the transmembrane pore region, where open-channel blockers typically bind, is predominantly composed of hydrophobic residues (Figure 1A) (17, 19).

We report here the single-channel kinetic characterization of a series of poly(ethylene glycol) (PEG)-based bis(trimethylammonium) salts (**1a–4**, Figure 2). A number of quaternary ammonium (QA) salts have been reported as agonists and/or open-channel blockers of the AChR (Figure 1B) (7, 20–23). Decamethonium, one of the best known blockers for the AChR, is composed of two trimethylammonium groups joined by a decamethylene spacer (Figure 1B) (22). We therefore prepared a series of prototype molecules through tethering two trimethylammonium groups with PEG spacers of varying size (Figure 2, compounds **1a–4**). PEG was chosen as the spacer scaffold due to its structural flexibility, synthetic versatility, and commercial availability of a wide range of molecular weights. To evaluate the effect of bivalency on blockade, a monovalent homologue of **1a** (compound **1b**, Figure 2) was also prepared and tested.

Blockade was examined at the single-molecule level using patch-clamp techniques. Except for the longest compound (**4**), all of the tested molecules function as both agonists and blockers of the AChR. Kinetic analysis of single-channel events indicates that both the association and dissociation rate constants decrease with increasing spacer length within the series **1a–3**. The decrease in association rate constant appears to result from the entropic cost of partitioning the polymer into the transmembrane lumen, while the drop in dissociation rate constant appears to be associated with weak, additive interactions between PEG and the channel. The



compound name	n	MW of the precursor PEG	$R_F$ (Å)
1a	2	194	8.0
2	6	370	12.2
3	~11	~590	16.3
4	~20	~1000	22.4



compound name	n	MW of the precursor PEG	$R_F$ (Å)
1b	2	194	8.0

FIGURE 2: Structure and estimated size of the TMA-PEG conjugates. The size of each precursor PEG is estimated as the Flory radius ( $R_F = aN^{0.6}$ ,  $a = 3.5$  Å for PEG) (15).

results support our design strategy and provide insight into the future design of kinetically tunable channel blockers.

## MATERIALS AND METHODS

**Synthesis.** Compounds **1a**, **1b**, **2**, **3**, and **4** were synthesized as described in the Supporting Information. The purity and the structure of products were confirmed by NMR ( $^1\text{H}$  and  $^{13}\text{C}$ ) and high-resolution electrospray mass spectrometry.

**Plasmids and Channel Expression.** The cDNA clones of adult mouse muscle AChR subunits ( $\alpha$ ,  $\beta$ ,  $\delta$ ,  $\epsilon$ ) in the vector pRBG4 were generously provided by Professor Anthony Auerbach (SUNY Buffalo, Buffalo, NY) (24). The  $\alpha$  subunit contains the previously described V433A background mutation, which does not affect gating kinetics and is referred to as wild-type (24). Plasmids were transiently transfected into HEK-293 human embryonic kidney cells (ATCC CRL-1573) by calcium phosphate precipitation (24). In brief, HEK-293 cells were maintained in Dulbecco's minimum essential media (DMEM) (Invitrogen, Carlsbad, CA) supplemented with 10% fetal bovine serum (FBS) (Invitrogen) at 37 °C and 5%  $\text{CO}_2$ . Cells were plated 24 h before transfection to reach a confluence of 40–60%. A total of 3.5  $\mu\text{g}$  of DNA per 35 mm culture dish in the ratio of 2:1:1:1  $\alpha$ : $\beta$ : $\delta$ : $\epsilon$ ) was used. The medium was changed 24 h after the addition of DNA, and patch-clamp recordings were performed 20–36 h thereafter.

**Electrophysiology.** Single-channel currents from adult mouse muscle AChRs were recorded using patch-clamp techniques in the cell-attached configuration. Unless otherwise specified, a holding potential of +70 mV was applied. Patch pipets were pulled from borosilicate capillary tubes (World Precision Instruments, Sarasota, FL) and were coated with Sylgard 184 (Dow Corning, Midland, MI). Pipet resistances were typically 10–20 M $\Omega$ . The extracellular solution (bath solution) comprised (mM) 137.9 NaCl, 8.1  $\text{Na}_2\text{HPO}_4$ , 2.7 KCl, 1.5  $\text{KH}_2\text{PO}_4$ , 0.9  $\text{CaCl}_2$ , and 0.5  $\text{MgCl}_2$  (pH 7.4). The pipets were filled with the bath solution supplemented with the small molecule of interest. The currents were amplified (Axopatch 200B; Axon Instruments, Foster City, CA), low-pass filtered at 10 kHz, and digitized at 20 kHz (NI 6040 E Data Acquisition Board; National Instruments, Austin, TX). Data were recorded directly to a

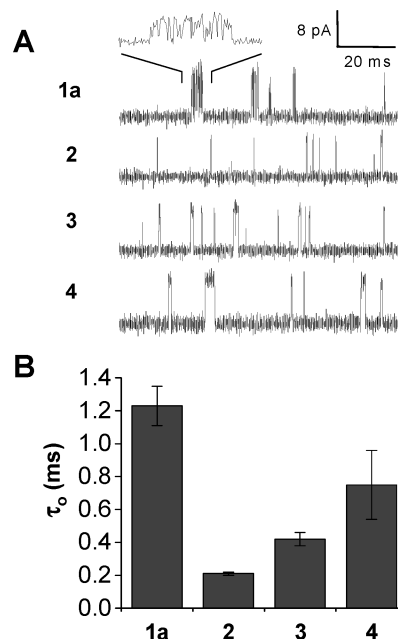


FIGURE 3: Single-channel identifications of the TMA-PEG conjugates. (A) Representative traces at 100  $\mu\text{M}$  **1a**, **2**, **3**, and **4** (holding potential = +70 mV). Currents are presented as upward deflections. (B) The apparent mean open time ( $\tau_o$ ) of the AChR at 100  $\mu\text{M}$  of each tested compound. Error bars represent standard deviations of triplicates.

desktop PC hard drive using the QuB software (www.qub.buffalo.edu).

**Data Analysis.** Kinetic analysis of single-channel currents was carried out using the QuB suite (25, 26). Current records from membrane patches with relatively low channel activity (defined here as patches containing fewer than four channels open simultaneously at any point during the record) were used for analysis. The currents were idealized using the segmented k-means (SKM) hidden Markov algorithm at full bandwidth (10 kHz) (27). Kinetic modeling of the idealized intervals was performed using the maximum interval likelihood (MIL) method (25, 26). The dead time was set as 0.125 ms for the following model in MIL:



where C, O, and OB refer to the closed, open, and blocked states of the AChR and  $\beta$ ,  $\alpha$ ,  $k_{+B}$ ,  $k_{-B}$ , and [B] refer to channel opening rate, channel closing rate, blocker association rate constant, blocker dissociation rate constant, and blocker concentration, respectively. At higher blocker concentrations (mostly higher than 200  $\mu\text{M}$ ) or when the channel activity is very low, a third closed state was often required for reasonable fitting. For compounds **2** and **3**, the values of  $\alpha$ ,  $\beta$ ,  $k_{+B}[\text{B}]$ , and  $k_{-B}$  were obtained directly from MIL fitting. The  $\alpha$  and  $k_{+B}$  values extracted from MIL fitting (Supporting Information Figure S1) are comparable with those estimated from the time constant for open dwells (Figure 4A and eq 4). For compound **4**, the closed dwells can be well-fitted by a single exponential distribution without the addition of blocked state (OB) in MIL fitting.

In the presence of **1a** or **1b**, the single-channel currents represent bursts of brief opening events separated by short gaps (Figure 3A). In most data records, the short gaps within bursts of openings could be partially resolved at our recording

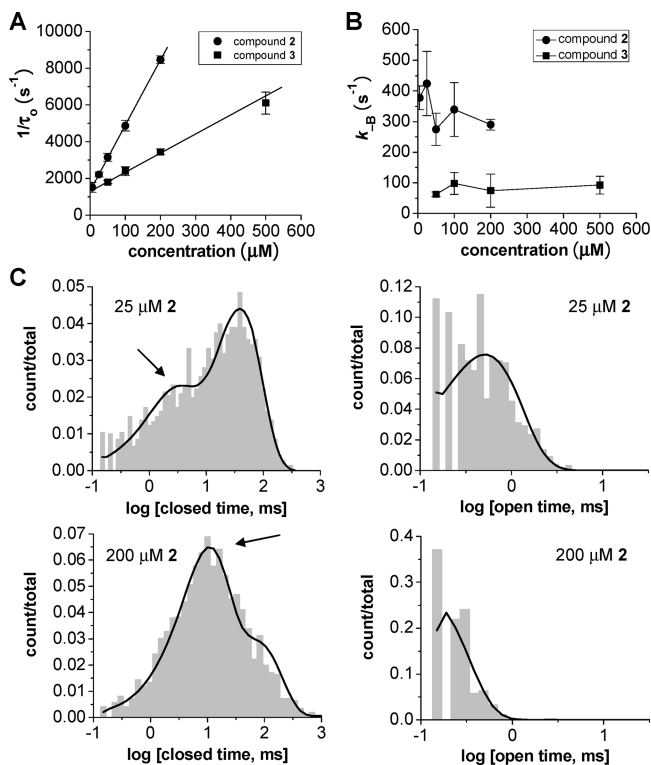


FIGURE 4: (A) Increase of  $1/\tau_o$  as a function of blocker concentration. Data were fitted by least-squares linear regression. (B) The dissociation rate constant ( $k_{-B}$ ) of compounds **2** and **3** at various concentrations. (C) Representative histograms of closed- and open-time distributions at low and high concentrations of compound **2**. Arrows indicate the closed-time components corresponding to the “blocked” state. A holding potential of +70 mV was applied in all recordings. Error bars represent standard deviations of triplicates.

bandwidth, and a fast component (lifetime < 1 ms) could be found in the closed-time distribution. The time constant ( $\tau$ ) and the area ( $a$ ) of this fast component and its closest slow component were used to calculate the critical time constant ( $\tau_c$ ) for defining bursts of openings (28). Bursts of openings were defined using  $\tau_c$  as the shortest gap duration between two bursts. At 1 mM **1a**, the events were too fast to be resolved, and the fast component could not be found in the closed-time distribution. A fixed  $\tau_c$  (1 ms) was used to define bursts in such files. Recording segments containing 1500–15000 single-channel opening bursts were chosen for further analysis.

Power spectra for single-channel records were obtained using the QuB suite. The net power spectrum, which is a measurement of the excess current noise when the channel is equilibrating between open and blocked states, was plotted by subtracting the spectral density function of the background noise from that of the open channels (29). The resulting net spectrum (plotted within a range of 500–10000 Hz) was fitted to a Lorentzian distribution:

$$S(f) = \frac{S(0)^2 f_c^2}{f^2 + f_c^2} \quad (2)$$

where  $S(f)$  is the spectral density function,  $f$  is the frequency, and  $f_c$  is the half-amplitude frequency (i.e., corner frequency). The association and dissociation rate constants were calculated from the linear dependence of  $f_c$  on blocker concentration (29):

$$f_c = \left( \frac{k_{-B}}{2\pi} \right) + \left( \frac{k_{+B}}{2\pi} \right) [B] \quad (3)$$

For the analysis of voltage-dependent blockade by **1a** and **1b**, fractional blockade was defined by comparing the mean current amplitude ( $i_{\text{mean}}$ ) and the current amplitude of the unblocked state ( $i_{\text{unblock}}$ ) for the bursts (29). The value of  $i_{\text{mean}}$  was obtained directly from SKM. The value of  $i_{\text{unblock}}$  was defined as the amplitude corresponding to the “open state” peak in the amplitude histogram plotted for bursts of single-channel openings (see Figure 6C for representative histograms). The membrane potential ( $V_m$ ) at a given holding potential ( $V_{\text{hold}}$ ) was estimated as  $V_{\text{rest}} - V_{\text{hold}}$ , where  $V_{\text{rest}}$  (resting potential) is the membrane potential in the absence of externally applied voltage. The reversal potential (the transmembrane voltage at which the direction of current starts to reverse) was assumed to be 0 mV (30), and  $V_{\text{rest}}$  was estimated by plotting  $i_{\text{unblock}}$  as a function of  $V_{\text{hold}}$  and measuring the  $x$ -intercept of the best-fit line.

## RESULTS

*Characterization of Single-Channel Currents Induced by PEG-Linked Bis(trimethylammonium) Compounds.* Several cationic organic compounds containing one or more trimethylammonium headgroups exhibit both agonist and blocker activities (20–23). For instance, decamethonium and phenylpropyltrimethylammonium (PPTMA) have been characterized as weak agonists of the AChR with moderate affinities for the open pore ( $K_d$  values are 9–20 and 90–160 μM, respectively) (22). These compounds cause a decrease in the apparent mean open time ( $\tau_o$ ) in a dose-dependent manner. Smaller compounds, such as acetylcholine (ACh) or carbamylcholine (CCh), exhibit fast blockade kinetics (20, 29). Blockade by these small molecules leads to bursts of single-channel currents (which are composed of brief, partially resolved conducting and blockade events) and reduced mean current amplitude. Compounds **1a–4** were hypothesized to act analogously to these previously characterized agonists/blockers.

To determine whether compounds **1a–4** act as agonists and/or channel blockers, we measured single-channel currents of the AChR in the presence of each compound at a concentration of 100 μM (Figure 3). As predicted, all of the compounds are capable of inducing channel openings. However, the recording traces (Figure 3A) show that these molecules exhibit distinct behaviors. The smallest compound, **1a**, induces bursts of flickering events, indicating fast channel blockade. Compounds **2** and **3** do not cause well-defined bursts of opening events, but the  $\tau_o$  values at 100 μM **2** or **3** are relatively short ( $0.21 \pm 0.01$  and  $0.42 \pm 0.04$  ms, respectively; Figure 3B). In the absence of blockade, the mean duration of opening events stimulated by an agonist is defined as the reciprocal of the channel closing rate constant ( $\alpha$ ); we designate the  $\tau_o$  in the absence of blockade as “intrinsic  $\tau_o$ ” to distinguish it from the measured apparent  $\tau_o$ . A comparison of the intrinsic  $\tau_o$ s of TMA, decamethonium, and PPTMA (which are 0.66, 0.48, and 0.88 ms, respectively) (31, 22) indicates that the attachment of a spacer or other scaffolds to the TMA moiety does not have a large effect on intrinsic  $\tau_o$ . Therefore, the brevity of  $\tau_o$  measured at 100 μM of compound **2** or **3** is likely due to channel blockade by these molecules.

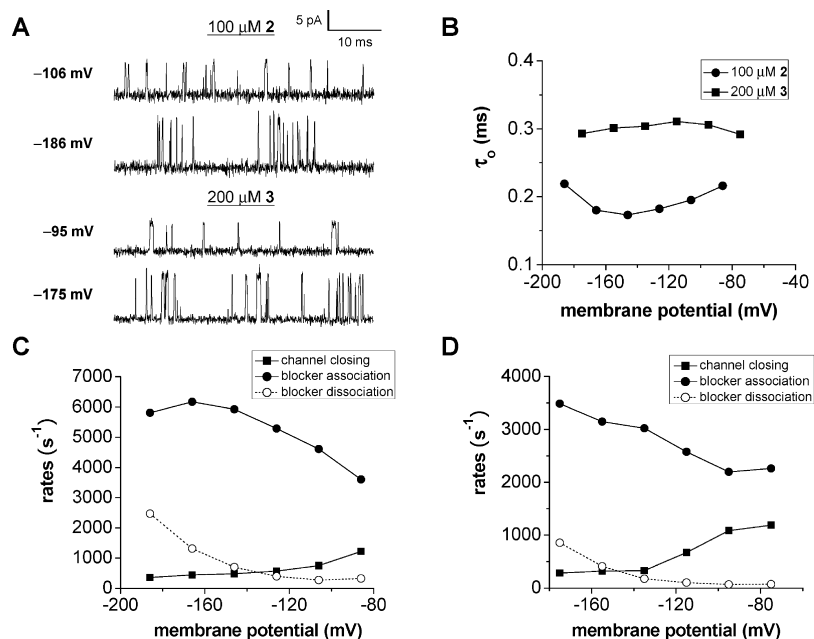


FIGURE 5: Voltage-dependent blockade by compounds **2** and **3**. (A) Representative traces. Currents are presented as upward deflections. (B) The change of apparent mean open time ( $\tau_o$ ) with membrane potential. (C, D) Voltage dependence of blockade kinetics at 100  $\mu\text{M}$  compound **2** (C) and 200  $\mu\text{M}$  compound **3** (D). Key: filled square, channel closing rate ( $\alpha$ ); filled circle, blocker association rate ( $k_{+B}[B]$ ); empty circle, blocker dissociation rate ( $k_{-B}$ ). One representative file for each condition is presented.

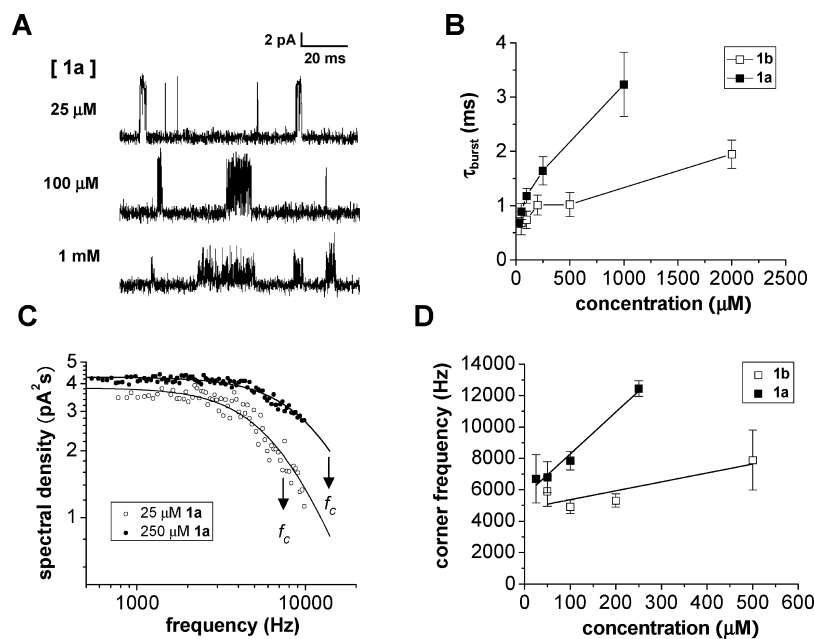


FIGURE 6: Concentration-dependent blockade by **1a** and **1b**. (A) Representative recording traces at various concentrations of **1a** (holding potential = +70 mV). Currents are presented as upward deflections. (B) Mean burst length ( $\tau_{\text{burst}}$ ) as a function of blocker concentration. (C) Representative net power spectra of current noise. Data are fitted by a single Lorentzian distribution.  $f_c$ , half-amplitude frequency (corner frequency). (D) Corner frequency as a function of blocker concentration. Data are fitted by least-squares linear regression. The slope and y-intercept correspond to  $k_{+B}/2\pi$  and  $k_{-B}/2\pi$ , respectively. Error bars represent standard deviations of triplicates.

The effects of compounds **1a–3** appear to be specific for QA-PEG conjugates of relatively low molecular weight. Treating the AChR with TMA and PEG-200, PEG-400, or PEG-600 produces openings that are free of flickering currents or shortened  $\tau_o$  observed for **1a–3** (data not shown). In addition, neither flickering currents nor reduced  $\tau_o$  values were observed at 100  $\mu\text{M}$  compound **4** ( $0.75 \pm 0.21$  ms, Figure 3) or larger congeners (data not shown), suggesting that QA molecules with long spacers (MW of PEG  $\geq 1000$ ) function only as agonists of the AChR. The effects observed with compounds **1a**, **2**, and

**3** are indicative of open-channel blockade by these QA-PEG conjugates. To test this hypothesis, we characterized concentration and voltage dependences of these compounds' effects on AChR currents.

**Mechanistic Studies on Blockade by Compounds 2 and 3.** The observed decrease in  $\tau_o$  values suggests that compounds **2** and **3** might act as blockers of the open AChR. Classical open-channel blockade (eq 1) conforms to the following predictions: (1)  $\tau_o$  decreases with increasing concentration of the blocker ( $[B]$ ); (2) mean duration of the blocked state ( $\tau_B$ ) is independent of  $[B]$ , and the dissociation rate constant

( $k_{-B}$ ) is the reciprocal of  $\tau_B$ ; and (3) blockade kinetics are voltage-dependent (due to blocker binding within the trans-membrane electric field) (7). To evaluate these predictions for AChR blockade by compounds **2** and **3**, we fitted the single-channel data to the sequential kinetic model (eq 1) at various concentrations of each compound. In the sequential blockade model, the concentration dependence of  $\tau_o$  can be described as

$$\frac{1}{\tau_o} = \alpha + k_{+B}[B] \quad (4)$$

where  $\alpha$  is the closing rate constant of the channel in the absence of blockade and  $k_{+B}$  is the association rate constant of the blocker.

As shown in Figure 4A, a linear relationship between  $1/\tau_o$  and  $[B]$  is observed for both **2** and **3**. The values of  $k_{+B}$  and  $\alpha$  are given by the slope and y-intercept, respectively, of the linear fits. The  $k_{+B}$  values for compounds **2** and **3** are  $36 \pm 1$  and  $10 \pm 1 \mu\text{M}^{-1} \text{s}^{-1}$ , respectively. The values of intrinsic  $\tau_o$ , defined as  $1/\alpha$ , are  $0.75 \pm 0.01$  and  $0.77 \pm 0.07$  ms for compounds **2** and **3**, suggesting that these compounds have agonist properties similar to those of TMA. Moreover, the intrinsic  $\tau_o$  for compounds **2** and **3** are very close to the  $\tau_o$  measured at  $100 \mu\text{M}$  compound **4** ( $0.75 \pm 0.21$  ms, Figure 3), suggesting that compound **4** does not induce significant blockade at this concentration.

In addition to  $\tau_o$ , the closed-time distribution also changes in a concentration-dependent manner (Figure 4C for compound **2** and Supporting Information Figure S2 for compound **3**). As shown in Figure 4C, the closed-time distribution is composed of two exponential components. The faster component has a relatively constant lifetime of 2–4 ms within the tested concentration range, whereas the lifetime of the slower component varies with the channel activity. In addition, the fast component represents a greater fraction of the total closing events as the concentration of compound **2** increases. Both observations suggest that the fast component represents the blocked state of the AChR. In the context of the sequential blockade mechanism (eq 1), the blocker dissociation rate constant ( $k_{-B}$ ) is the reciprocal of the mean blocked time ( $\tau_B$ ). Because  $k_{-B}$  is fairly constant over the tested concentration range (Figure 4B), a mean value is calculated for compound **2** ( $339 \pm 78 \text{s}^{-1}$ ). Similar blockade behavior is also observed with compound **3** (Figure 4B and Supporting Information Figure S2), and the mean value of  $k_{-B}$  for compound **3** is  $82 \pm 34 \text{s}^{-1}$ .

The concentration dependences of  $\tau_o$  and  $k_{-B}$  are both consistent with the predictions for open-channel blockade. We therefore went on to examine the voltage dependence of blockade kinetics. Although  $\tau_o$  does not show a significant voltage dependence for compound **2** or **3** (Figure 5B),  $\alpha$ ,  $k_{+B}[B]$ , and  $k_{-B}$  clearly exhibit changes with membrane potential for both blockers (Figure 5C,D). Compounds **2** and **3** share similar trends in these rates. The increase of intrinsic  $\tau_o$  (i.e., the decrease of  $\alpha$ ) with hyperpolarizing (i.e., more negative) membrane potential has been reported for the AChR (30), and we see the same trend in  $\alpha$  with both **2** and **3**. The blocker association rate, which is defined as  $k_{+B}[B]$  in the sequential blockade model, increases with hyperpolarizing membrane potential. Since  $[B]$  is constant during the measurements ( $100 \mu\text{M}$  for compound **2** and  $200 \mu\text{M}$  for compound **3**), the observed trend is in fact the voltage

dependence of  $k_{+B}$  for these blockers. For positively charged molecules, increasing  $k_{+B}$  with hyperpolarizing membrane potential is indicative of open-channel blockade from the extracellular side of the channel. Moreover, since blocker association generally reduces  $\tau_o$ , the lack of voltage dependence in  $\tau_o$  is presumably due to offsetting effects of  $k_{+B}$  and  $\alpha$ .

There is only a marginal variation in  $k_{-B}$  with voltage when the membrane potential is less negative than  $-120$  mV. At more hyperpolarizing membrane potentials, a more significant increase in  $k_{-B}$  can be observed (Figure 5C,D). A faster blocker dissociation rate leads to a shorter mean duration of the “blocked” state of the channel, which can be identified from the shift of the fast component in the closed-time distribution (Supporting Information Figure S3). At more negative membrane potentials, the closed and blocked states of the AChR are more kinetically distinguishable, which allows direct visualization of “burst-like” opening events (Figure 5A). The cause of increasing  $k_{-B}$  with membrane hyperpolarization is not yet clear: it might be permeation of the blocker into the cell (32, 33) or faster release of the blocker into the extracellular solution (due to the destabilization of blocker-channel interaction). In summary, the results suggest that, in addition to being agonists, compounds **2** and **3** also function as open-channel blockers of the AChR.

**Mechanistic Studies on Blockade by Compound 1a.** The flickering, burst-like single-channel currents stimulated by **1a** are indicative of fast open-channel blockade. In contrast to the longer lived blockade observed for **2** and **3**, gaps between brief opening events stimulated by **1a** can only be partially resolved at our recording bandwidth (Figure 3A). Several open-channel blockers of the AChR, such as TEA and PIP, are known to operate via this mechanism (23, 12). To further characterize the blockade mechanism, we measured single-channel currents at various concentrations of **1a** (Figure 6). When blocking and unblocking processes are fast, blocker binding may, counterintuitively, prolong bursts of channel openings, with higher concentrations of blocker producing longer bursts (7). The burst-like currents arise from repeated transient interruptions of ion conduction by blockade events when a channel is open. The duration of a burst is therefore the sum of the time that an open channel stays unblocked and the time that it is occupied by a blocker. If blocker binding does not accelerate the closure of an open channel, an increase in blocker concentration will lead to a higher frequency of blockade, resulting in a longer mean burst length. Experimentally, as the concentration of **1a** is increased, the frequency of brief interruptions of open-state currents, the reduction in mean conductance, and the mean duration of single-channel bursts all increase. As shown in Figure 6B, **1a** causes a concentration-dependent increase in mean burst duration ( $\tau_{\text{burst}}$ ), which is consistent with the prediction for fast open-channel blockade.

Because blocking and unblocking events are too fast to be measured directly,  $k_{+B}$  and  $k_{-B}$  were estimated through noise analysis, which has previously been used to study rapid channel blockade (29). When the concentration of **1a** increases, there is a decrease in the mean amplitude of the open-state current, which is accompanied by an increase in variance. Rapid blocking and unblocking events manifest themselves as noise in open-channel currents, allowing

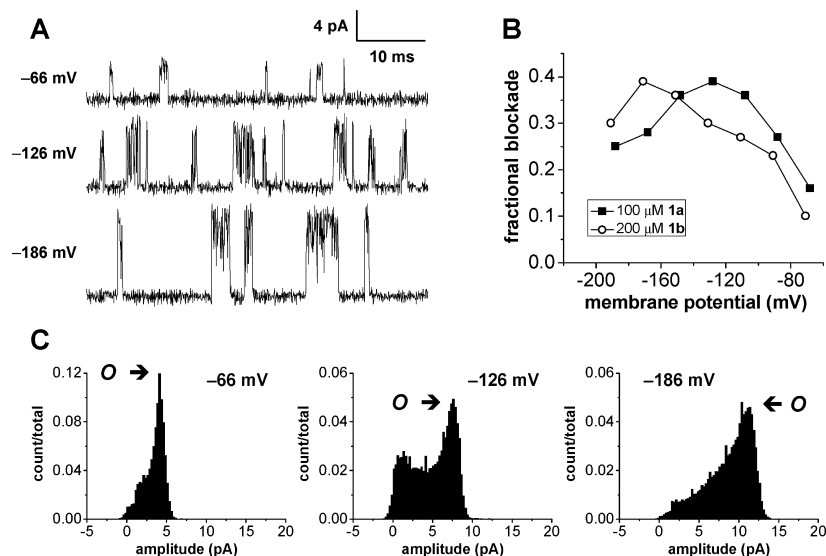


FIGURE 7: Voltage-dependent blockade by **1a** and **1b**. (A) Representative recording traces at various membrane potentials (100  $\mu\text{M}$  **1a**). Currents are presented as upward deflections. (B) Fractional blockade as a function of membrane potential. One representative patch out of triplicates is shown for each condition. (C) Representative amplitude histograms (plotted for single-channel bursts, 100  $\mu\text{M}$  **1a**) at various membrane potentials. Symbol "O" indicates the "open-state" peak.

blocking and unblocking rate constants to be determined from the power spectra of open channel noise (eqs 2 and 3; Figure 6C,D). From linear fitting of the dependence of  $f_c$  (the half-amplitude frequency of the net power spectrum) on [B], the  $k_{+B}$  and  $k_{-B}$  values are calculated to be  $168 \pm 17 \mu\text{M}^{-1} \text{s}^{-1}$  and  $(3.53 \pm 0.23) \times 10^4 \text{s}^{-1}$ , respectively (Figure 6D). The  $K_d$  is therefore  $210 \pm 25 \mu\text{M}$ . The rate constants are of the same order of magnitude as those of open-channel blockade by ACh, CCh, and PIP (29, 12).

To examine whether **1a** targets the transmembrane lumen of the AChR, blockade was measured at various membrane potentials. If **1a**, like compounds **2** and **3**, binds the open pore from the extracellular side, blockade would be favored at more negative membrane potentials. As predicted, channel blockade by **1a** (as measured in fractional blockade) is sensitive to alterations in the membrane potential (Figure 7). At 100  $\mu\text{M}$  **1a**, fractional blockade increases about 2.5-fold when the membrane potential goes from approximately  $-70$  to  $-130$  mV, suggesting that the positively charged **1a** is attracted by the transmembrane electric field. This observation is consistent with the prediction for blockade from the extracellular side. At membrane potentials more negative than  $-130$  mV, hyperpolarization causes a decrease in AChR blockade. The drop in fractional blockade might be a result of either increasing  $k_{-B}$  or decreasing  $k_{+B}$ . The voltage dependence of blockade by compounds **2** and **3** (Figure 5C,D) suggests that highly hyperpolarized membrane potentials are more likely to increase  $k_{-B}$  than to decrease  $k_{+B}$ . Combined with the observation of concentration-dependent increases in  $\tau_{\text{burst}}$  and open-state noise, the results support a mechanism in which **1a** binds transiently within the transmembrane lumen and impedes ion conductance through the open AChR.

**Effect of Valency on AChR Blockade.** All of the PEG-based blockers characterized above have two trimethylammonium groups per molecule. To investigate whether bivalency is a structural determinant for open-channel blockade, a monovalent homologue (**1b**) of **1a** was also characterized. Like **1a**, **1b** stimulates flickering AChR currents that can only be partially resolved at our recording

Table 1: Rate and Equilibrium Dissociation Constants for the PEG-Based Blockers

compound (PEG size)	$\alpha$ ( $\text{s}^{-1}$ ) <sup>a</sup>	$k_{+B}$ ( $\mu\text{M}^{-1} \text{s}^{-1}$ ) <sup>b</sup>	$k_{-B}$ ( $\text{s}^{-1}$ ) <sup>c</sup>	$K_d$ ( $\mu\text{M}$ ) <sup>d</sup>
<b>1a</b> (8.0 Å)		$168 \pm 17$	$(3.53 \pm 0.23) \times 10^4$	$210 \pm 25$
<b>2</b> (12.2 Å)	$1340 \pm 19$	$36 \pm 1$	$339 \pm 78$	$9 \pm 2$
<b>3</b> (16.3 Å)	$1300 \pm 116$	$10 \pm 1$	$82 \pm 34$	$8 \pm 3$
<b>1b</b> (8.0 Å)		$37 \pm 15$	$(3.01 \pm 0.40) \times 10^4$	$848 \pm 358$

<sup>a</sup> Channel closing rate constants ( $\alpha$ ) were estimated from the y-intercept of linear plots of  $1/\tau_o$  vs [B] (Figure 4A). <sup>b</sup> Blocker association rate constants ( $k_{+B}$ ) of **1a** and **1b** were obtained from noise analysis (Figure 6D). Values of  $k_{+B}$  for **2** and **3** were estimated from the slope of linear plots of  $1/\tau_o$  vs [B] (Figure 4A). <sup>c</sup> Blocker dissociation rate constants ( $k_{-B}$ ) of **1a** and **1b** were obtained from noise analysis (Figure 6D). For **2** and **3**, values of  $k_{-B}$  estimated from MIL fitting at various blocker concentrations were pooled for calculation (Figure 4B). The mean  $\pm$  standard deviation values from 20 and 12 patches are reported for **2** and **3**, respectively. <sup>d</sup> The equilibrium dissociation constant ( $K_d$ ) for the blocker is defined as  $k_{-B}/k_{+B}$ .

bandwidth (data not shown). We therefore analyzed blockade kinetics using the same methods as those applied for the analysis of **1a** (Figure 6B,D). As shown in Figure 6B, **1b** also causes a concentration-dependent increase in  $\tau_{\text{burst}}$ , but the effect is smaller than that observed with **1a**. The comparison of blockade kinetics between **1a** and **1b** (Table 1) shows that **1a** binds the open AChR approximately 5-fold faster than **1b** does. There is, however, only a marginal difference in the dissociation rate constant, leading to a 4-fold decrease in blocker's affinity ( $K_d = 848 \pm 358 \mu\text{M}$ ). Although a direct determination of  $\alpha$  was not available for **1a** or **1b**,  $\tau_o$  values are similar at low [**1a**] or [**1b**] (0.77 ms at 5  $\mu\text{M}$  **1a** and 0.79 ms at 10  $\mu\text{M}$  **1b**; data not shown), suggesting that the intrinsic  $\tau_o$  is not affected by the number of QA groups attached to PEG. These observations suggest that the shorter  $\tau_{\text{burst}}$  observed with **1b** is the consequence of the reduction in blockade frequency.

Supporting the hypothesis that compound **1b** binds to the open channel, fractional blockade by this compound is sensitive to membrane potential changes (Figure 7B). Consistent with the observations for  $k_{+B}$  and  $K_d$ , the decreased valency of **1b** is associated with more than a 2-fold

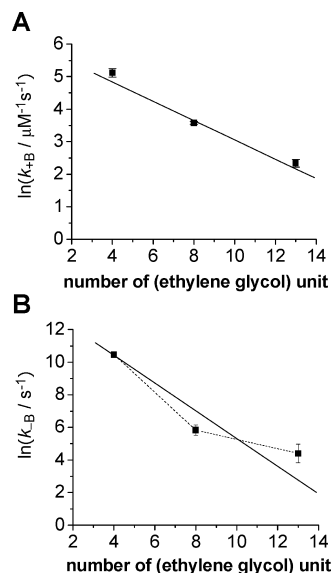


FIGURE 8: Dependence of  $\ln(k_{+B})$  (A) and  $\ln(k_{-B})$  (B) on spacer size (expressed as the number of ethylene glycol units). The solid lines are least-squares linear fits.

difference in fractional blockade. Comparing fractional blockade at 100  $\mu\text{M}$  **1a** and 200  $\mu\text{M}$  **1b**, **1a** remains a stronger blocker over the less hyperpolarized membrane potentials ( $-70$  to  $-130$  mV), indicating that the additional QA group of **1a** might have other effects on AChR blockade in addition to doubling the effective blocker concentration.

**Effect of Spacer Size on AChR Blockade.** The rate constants ( $\alpha$ ,  $k_{+B}$ , and  $k_{-B}$ ) and equilibrium dissociation constant ( $K_d$ ) determined above are summarized in Table 1. In the series comprising compound **1a** through compound **3**, each extension of the PEG backbone leads to an  $\sim 4$  Å increase in the length (estimated from the Flory radius of the precursor PEG). The channel closing rate constant ( $\alpha$ ) of the AChR appears to be unaffected by the size of these bivalent compounds. Although we did not perform a direct measurement of  $\alpha$  for **1a** and **1b**, an approximate measurement of  $\alpha$  from recordings at low concentrations (5  $\mu\text{M}$  for **1a** and 10  $\mu\text{M}$  for **1b**, where fractional blockade is less than 10%) gives values around 1300  $\text{s}^{-1}$  for these compounds, which are close to the values observed for compounds **2** and **3**. Both  $k_{+B}$  and  $k_{-B}$  are inversely correlated with PEG size (Table 1 and Figure 8). Using **1a** as a reference compound, the addition of four and nine ethylene glycol units causes 4.7- and 16-fold decreases in  $k_{+B}$ , respectively. The trend in  $k_{-B}$  is more dramatic: the addition of four and nine ethylene glycol units leads to 100- and 430-fold decreases in  $k_{-B}$ , respectively. The differential PEG length sensitivity of  $k_{+B}$  and  $k_{-B}$  results in a significant enhancement of binding affinity for both **2** and **3** compared to **1a**. It is worth noting that, although compounds **2** and **3** exhibit distinct blockade kinetics, their binding affinities are similar at equilibrium (Table 1).

## DISCUSSION

In the present study, the kinetics and thermodynamics of channel blockade by QA-PEG conjugates were investigated. For symmetric, bivalent blockers (**1a–3**), varying the length of the PEG spacer between two QA groups leads to systematic changes in the blocker association and dissociation

rate constants. Presence of two QA groups per molecule is not a critical structural determinant for PEG-based blockers, but bivalency appears to enhance the frequency of blocker binding to the open pore. Implications for future design of polymer-based, kinetically tunable blockers will be discussed.

**Mechanism of Blockade.** The results of electrophysiological studies suggest that compounds **1a**, **1b**, **2**, and **3** all function as open-channel blockers of the AChR. For compounds **2** and **3**, the dose-dependent reduction in  $\tau_o$  and the presence of a faster kinetic component (which has a fairly constant lifetime over the tested concentration range) in the closed-time distribution are in good agreement with the sequential blockade mechanism (eq 1). Compounds **1a** and **1b** do not reduce  $\tau_o$  but instead cause burst-like flickering events and increased current noise. The dose-dependent increase in  $\tau_{\text{burst}}$  observed with **1a** and **1b** suggests fast blocking and unblocking of the open channel by these compounds. The voltage dependence of AChR blockade by compounds **1a**, **1b**, **2**, and  $\mathbf{3}$  further supports a mechanism in which these molecules block the open pore of the channel. In general, blockade is sensitive to changes in the membrane potential when a charged blocker binds within the transmembrane electric field. The voltage dependence of blockade can be used to obtain a rough estimate of the location in which blocker binds within the transmembrane lumen. For fast blockade by **1a**, the electric distance  $\delta$  (i.e., the fraction of total transmembrane potential drop measured from the extracellular side of the membrane to the blocker binding site) can be estimated using the Woodhull model, yielding a value of  $0.32 \pm 0.05$  (Supporting Information Figure S4) (34, 20, 12). Because a clear voltage-dependent increase in  $k_{+B}$  with hyperpolarization is observed for compounds **2** and **3**, the  $\delta$  values for these blockers can be estimated according to the Eyring rate equation (12, 35). By linear fitting of the plot of  $\ln(k_{+B})$  vs membrane potential,  $\delta$  can be calculated as  $0.25 \pm 0.06$  and  $0.19 \pm 0.07$  for compounds **2** and **3**, respectively, from the slope (Supporting Information Figure S5). Assuming a membrane thickness of 40 Å, the binding sites of **1a**, **2**, and **3** are  $13 \pm 2$ ,  $10 \pm 2$ , and  $7 \pm 3$  Å from the extracellular side of the membrane, respectively.

Compounds **1a–3** are weak agonists of the AChR in addition to being channel blockers. However, the structure of the AChR suggests that binding to the agonist binding site and to the transmembrane lumen are independent processes. The agonist binding sites are  $\sim 40$  Å above the cell membrane (Figure 1A) (18), suggesting that compounds **1a–3**, which have sizes of 8–16 Å (Figure 2), are unlikely to span the pore and the agonist binding site. The observed voltage-dependent blockade with these compounds also excludes a mechanism in which a bivalent molecule spans the two agonist binding sites and prevents ions from flowing through the vestibule tunnel. In such a mechanism, the positively charged blocker would act at a position distant from the transmembrane region and blockade would be expected to be insensitive to voltage changes, which is in contrast to our observations.

Blockade by **1b** suggests that having one QA moiety is sufficient for a PEG conjugate to block the AChR. However, incorporation of a second QA group (**1a**) further improves blocker affinity. Comparing  $K_d$ ,  $k_{+B}$ , and  $k_{-B}$  of **1a** and **1b**, we find that **1a** binds the AChR pore with 4-fold higher affinity than **1b** and that the difference in binding affinity

predominately comes from the blocker association rate constant. Although an increase in the effective concentration of the pore-binding moiety can contribute to this difference, the bivalency of **1a** produces only a 2-fold increase in  $[QA]$  over **1b**, which could account for a difference in  $k_{+B}$  of at most a factor of 2. An alternative explanation is that the additional QA group of **1a** increases the probability of productive binding with the AChR. Prior to pore blockade, the blockers may form short-lived preassociation complexes with the negatively charged extracellular vestibule. The higher charge density of **1a** might stabilize its residence in the vestibule, making productive collisions of **1a** with the pore more likely.

**Effect of Spacer Length on AChR Blockade.** The association rate constant for blockade decreases with increasing PEG length in the series of compounds **1a–3** (Table 1 and Figure 8A). This observation is indicative of an entropic barrier that prevents partitioning of bulky PEGs into the channel pore. Sulfhydryl-directed PEG reagents have been previously reported to partition into the pore of  $\alpha$ -hemolysin according to a simple scaling law (15). A linear relationship was found between the natural logarithm of the apparent rate constant ( $k'$ ) for a specific luminal cysteine residue and the number of ethylene glycol units ( $N$ ) in the PEG reagent. The slope of this linear correlation was  $-(a/D)^{5/3}$ , where  $a$  is the persistence length (i.e., effective monomer length) of the polymer and  $D$  is pore diameter. Analogously, the plot of  $\ln(k_{+B})$  vs  $N$  is linear for our PEG-based blockers (Figure 8A). Since blockers **1a–3** are smaller than the diameter of the vestibule tunnel (20–30 Å) (18) but larger than the pore diameter (7–8 Å) (36, 37), the entry of these molecules into the transmembrane pore is expected to contribute predominately to the entropic cost of blockade. Assuming a persistence length of 3.5 Å for PEG (15), a diameter of 7.1 Å is obtained according to slope =  $-(a/D)^{5/3}$ , which is in good agreement with the reported value for the pore diameter of the AChR (36, 37). The length dependence of  $k_{+B}$  for compounds **1a–3** therefore supports the hypothesis that the primary entropic barrier for blocker association is the partitioning of a polymeric scaffold into the transmembrane pore.

The dissociation rate constant is found to be inversely correlated with the length of PEG. Assuming that the interaction between the channel and each monomer unit is identical and additive, the activation energy for blocker dissociation can be estimated from

$$k_{-B} = A \exp\left(\frac{-E_{a(\text{total})}}{RT}\right) \cong A \exp\left(\frac{-NE_{a(\text{unit})}}{RT}\right) \quad (5)$$

where  $A$  is the proportionality constant,  $N$  is the number of ethylene glycol units, and  $E_{a(\text{total})}$  and  $E_{a(\text{unit})}$  are the overall activation energy for blocker dissociation and activation energy for dissociation per monomer unit, respectively. According to eq 5, the plot of  $\ln(k_{-B})$  vs  $N$  is linear with a slope of  $-(E_{a(\text{unit})}/RT)$ . Linear least-squares fitting suggests that each ethylene glycol unit contributes  $\sim 0.4$  kcal/mol of binding energy in the series **1a–3** (Figure 8B), although the correlation between the number of monomer units and the total binding energy may not be strictly linear (see discussion below).

By extrapolating the linear correlation between  $\ln(k_{+B})$  and  $N$  (Figure 8A),  $k_{+B}$  of compound **4** ( $N \sim 22$ ) is estimated to

be  $0.6 \mu\text{M}^{-1} \text{s}^{-1}$ . Using this estimate, the blocker association rate is predicted to be only  $0.06 \text{ ms}^{-1}$  at  $100 \mu\text{M}$  compound **4**. Since the intrinsic  $\tau_o$  for our QA-PEG conjugates are 0.7–0.8 ms, the probability of observing blockade events before the open AChR closes is expected to be very low under this condition (the relative frequency of blockade, defined as  $k_{+B}[B]/(\alpha + k_{+B}[B])$ , is  $\sim 0.05$  at  $100 \mu\text{M}$  compound **4**). Moreover, because the size of compound **4** ( $R_F = 22.4 \text{ \AA}$ ) is close to the diameter of the extracellular vestibule, the entropic cost for compound **4** to enter the vestibule should not be neglected. The concentration of PEG-1000 in a 20 Å wide chamber is  $\sim 30\%$  of that in the bulk solution according to the scaling law (15), giving an even lower  $k_{+B}$  for compound **4** than predicted from the scaling analysis in Figure 8A.

The value of  $k_{-B}$  is also likely to deviate from the predicted value (Figure 8B and eq 5) when  $N$  is large. For small PEG-based blockers, the interaction between the channel and each monomer unit is assumed to be identical and additive because these molecules may be fully confined in the transmembrane lumen, forming favorable interactions with the channel surface. For large congeners, however, the polymer size might exceed the space available for blocker binding within the pore, leading to higher  $k_{-B}$  values than predicted. Such a deviation might explain the observed length-dependent trend in  $k_{-B}$ : the drop in  $\ln(k_{-B})$  is steeper from  $N = 4$  to  $N = 8$  compared to the decrease from  $N = 4$  to  $N = 13$  (Figure 8B, dashed lines).

The blockade behavior of **1a–3** is similar to that of the previously reported PIP derivatives (12) in that there is a linear decrease in  $\ln(k_{-B})$  with increasing number of methylene groups in the alkyl tail. As proposed for the PIP derivatives, this effect is presumably due to differential hydrophobic and/or van der Waals interactions between each blocker and the nonpolar pore-lining residues of the AChR. Interestingly, however,  $k_{+B}$  for the PIP derivatives remains fairly constant without a particular trend over the range of alkyl chain length examined, which is in contrast to our observation with QA-PEG conjugates. Because changes in molecular size are much smaller for the PIP derivatives ( $R = \text{methyl to hexyl}$ ) than those for compounds **1a–3**, the entropic barrier for entry of these PIP derivatives is expected to depend only weakly on alkyl chain length over the range tested.

**Implications for the Design of Kinetically Tunable Blockers.** This model study demonstrates how QA-PEG conjugates block the open AChR in a structure-dependent manner. Both the spacer length and the number of attached QA groups affect the kinetics and thermodynamics of blockade. The association and dissociation rate constants each exhibit a characteristic dependence on spacer length, suggesting that it will be possible to create blockers with predictable blockade kinetics by adjusting the size of the polymer backbone. In terms of their binding kinetics and thermodynamics, blockers **1a–3** are comparable to the QA-based blockers that have previously been characterized (Supporting Information Table S1). Blockers **2** and **3** exhibit AChR binding affinities greater than the highest affinity alkyl-PIP blockers (12) and comparable to those of the well-known QA-based open-channel blockers such as decamethonium ( $K_d = 9\text{--}20 \mu\text{M}$ ) (22) and QX-222 ( $K_d \sim 30 \mu\text{M}$ ) (7). It is also worth noting that  $k_{+B}$  and  $k_{-B}$  of blockers **1a–3** span 1 and

2 orders of magnitude, respectively, and that these ranges cover the blockade rate constants of many previously characterized QA-based blockers (Supporting Information Table S1). The lowest dissociation rate constant observed (for compound **3**) is  $<100\text{ s}^{-1}$ , indicating that QA-PEG conjugates may have the potential of accelerating AChR current decays through long-lived interruption of channel openings.

Due to the lack of a high-resolution structure for the transmembrane lumen, the rational design of open-channel blockers for the AChR remains challenging. The observed length-dependent changes of blockade kinetics in this study suggest an alternative strategy for blocker design: when a flexible polymer scaffold is incorporated into the blocker structure, a systematic modulation of blocker association/dissociation may be achieved by modifying the size of the polymer scaffold. The ability to create a series of blocker congeners with a broad range of blockade kinetics would allow systematic modulation of the kinetics of AChR-mediated currents. Several blockers of the muscle-type AChR have also been reported to inhibit neuronal AChRs, indicating that PEG-based blockers are likely to target neuronal AChRs and function in a similar manner (38–42). In the long term, these blockers might be suitable for studying modulation of synaptic transmission in perfusable experimental preparations such as brain slices, which retain high degrees of neuronal connectivity and are commonly used in the study of physiological phenomena (e.g., synaptic plasticity). However, application of QA-PEG conjugates to neuronal AChRs may be restricted *in vivo*, since the access of these charged molecules to the central nervous system may be limited by the blood–brain barrier. Finally, PEG is also likely to serve as a useful scaffold for pore-directed blockers of channels other than the AChR, since the results of this study suggest that blockade properties are likely not to depend strongly on the details of pore structure.

Future work will focus on studying the effects of QA end groups on blockade kinetics and binding-site selectivity. The bivalent PEG-based blockers are designed to afford versatility in structural modifications. In addition to spacer length, the end groups can be modified in a fairly straightforward manner. Compounds **1a–4** were made from PEGs through a three-step conversion (Supporting Information Schemes S1 and S2). The trimethylammonium group used for compounds **1a–4** can be replaced with other QA moieties by the same synthetic strategy using the corresponding tertiary amines. Structural modifications of the QA moiety are likely to enhance blockade affinity of an open-channel blocker. For instance, when the trimethylammonium group of QX-222 is replaced with triethylammonium, the resulting blocker has a binding affinity  $\sim 30$ -fold greater than QX-222 itself (7). Moreover, replacement of the trimethylammonium group, which is shared by several AChR agonists, with other QA groups might allow the resulting QA-PEG conjugates to bind more selectively to the pore rather than the agonist binding site.

In summary, this study has demonstrated that simple QA salts based on a PEG scaffold can block the open AChR with reasonably good affinities and predictable kinetics that depend on the size of PEG spacer. Due to their length-dependent changes in blockade kinetics, PEG-based blockers

are potentially useful for the systematic modulation of synaptic currents in the studies of synaptic transmission.

## ACKNOWLEDGMENT

We thank Prof. Anthony Auerbach for providing plasmids and Profs. JoAnne Stubbe, Sarah O'Connor, and Barbara Imperiali for comments on an earlier version of the manuscript.

## SUPPORTING INFORMATION AVAILABLE

Detailed experimental procedures for the synthesis of compounds; estimation of  $k_{+B}$  and  $\alpha$  for compounds **2** and **3** by MIL fitting; representative histograms of closed- and open-time distributions at low and high concentrations of compound **3**; representative histograms of closed-time distributions at different membrane potentials in the presence of compound **2** or **3**; estimation of electric distance for compounds **1a–3**; values of  $k_{+B}$ ,  $k_{-B}$ , and  $K_d$  for other previously reported open-channel blockers of the AChR. This material is available free of charge via the Internet at <http://pubs.acs.org>.

## REFERENCES

- Bowman, W. C. (2006) Neuromuscular block. *Br. J. Pharmacol.* **147**, S277–S286.
- Foster, A. C., and Kemp, J. A. (2006) Glutamate- and GABA-based drugs: the next wave of CNS therapeutics? *Curr. Opin. Pharmacol.* **6**, 7–17.
- Wickenden, A. D. (2002)  $K^+$  channels as therapeutic drug targets. *Pharmacol. Ther.* **94**, 157–182.
- Bonci, A., Jr. (2005) Ion channels and intracellular signaling proteins as potential targets for novel therapeutics for addictive and depressive disorders. *Pharmacol. Ther.* **108**, 65–75.
- Cathala, L., Brickley, S., Cull-Candy, S., and Farrant, M. (2003) Maturation of EPSCs and intrinsic membrane properties enhances precision at a cerebellar synapse. *J. Neurosci.* **23**, 6074–6085.
- Juusola, M., Robinson, H. P. C., and de Polavieja, G. G. (2007) Coding with spike shapes and graded potentials in cortical networks. *BioEssays* **29**, 178–187.
- Neher, E., and Steinbach, J. H. (1978) Local anesthetics transiently block currents through single acetylcholine-receptor channels. *J. Physiol.* **277**, 153–176.
- Beam, K. G. (1976) A voltage-clamp study of effect of two lidocaine derivatives on time course of endplate currents. *J. Physiol.* **258**, 279–300.
- Sieb, J. P., Milone, M., and Engel, A. G. (1996) Effects of the quinoline derivatives quinine, quinidine, and chloroquine on neuromuscular transmission. *Brain Res.* **712**, 179–189.
- Fukudome, T., Ohno, K., Brengman, J. M., and Engel, A. G. (1998) AChR channel blockade by quinidine sulfate reduces channel open duration in the slow-channel congenital myasthenic syndrome. *Ann. N.Y. Acad. Sci.* **841**, 199–202.
- Harper, C. M., and Engel, A. G. (1998) Quinidine sulfate therapy for the slow-channel congenital myasthenic syndrome. *Ann. Neurol.* **43**, 480–484.
- Carter, A. A., and Oswald, R. E. (1993) Channel blocking properties of a series of nicotinic cholinergic agonists. *Biophys. J.* **65**, 840–851.
- Bezrukov, S. M., Vodyanoy, I., Brutyan, R. A., and Kasianowicz, J. J. (1996) Dynamics and free energy of polymers partitioning into a nanoscale pore. *Macromolecules* **29**, 8517–8522.
- Movileanu, L., Howorka, S., Braha, O., and Bayley, H. (2000) Detecting protein analytes that modulate transmembrane movement of a polymer chain within a single protein pore. *Nat. Biotechnol.* **18**, 1091–1095.
- Movileanu, L., and Bayley, H. (2001) Partitioning of a polymer into a nanoscopic protein pore obeys a simple scaling law. *Proc. Natl. Acad. Sci. U.S.A.* **98**, 10137–10141.
- Sine, S. M., and Engel, A. G. (2006) Recent advances in Cys-loop receptor structure and function. *Nature* **440**, 448–455.
- Karlin, A. (2002) Emerging structure of the nicotinic acetylcholine receptors. *Nat. Rev. Neurosci.* **3**, 102–114.

18. Unwin, N. (2005) Refined structure of the nicotinic acetylcholine receptor at 4 Å resolution. *J. Mol. Biol.* 346, 967–989.
19. Arias, H. R. (1998) Binding sites for exogenous and endogenous noncompetitive inhibitors of the nicotinic acetylcholine receptor. *Biochim. Biophys. Acta* 1376, 173–220.
20. Sine, S. M., and Steinbach, J. H. (1984) Agonists block currents through acetylcholine receptor channels. *Biophys. J.* 46, 277–284.
21. Grosman, C., and Auerbach, A. (2000) Asymmetric and independent contribution of the second transmembrane segment 12' residues to diliganded gating of acetylcholine receptor channels: a single-channel study with choline as the agonist. *J. Gen. Physiol.* 115, 637–651.
22. Marshall, C. G., Ogden, D., and Colquhoun, D. (1991) Activation of ion channels in the frog endplate by several analogs of acetylcholine. *J. Physiol.* 433, 73–93.
23. Akk, G., and Steinbach, J. H. (2003) Activation and block of mouse muscle-type nicotinic receptors by tetraethylammonium. *J. Physiol.* 551, 155–168.
24. Salamone, F. N., Zhou, M., and Auerbach, A. (1999) A re-examination of adult mouse nicotinic acetylcholine receptor channel activation kinetics. *J. Physiol.* 516, 315–330.
25. Qin, F., Auerbach, A., and Sachs, F. (1996) Estimating single-channel kinetic parameters from idealized patch-clamp data containing missed events. *Biophys. J.* 70, 264–280.
26. Qin, F., Auerbach, A., and Sachs, F. (1997) Maximum likelihood estimation of aggregated Markov processes. *Proc. R. Soc. London, Ser. B* 264, 375–383.
27. Qin, F. (2004) Restoration of single-channel currents using the segmental k-means method based on hidden Markov modeling. *Biophys. J.* 86, 1488–1501.
28. Clapham, D. E., and Neher, E. (1984) Substance P reduces acetylcholine-induced currents in isolated bovine chromaffin cells. *J. Physiol.* 347, 255–277.
29. Ogden, D. C., and Colquhoun, D. (1985) Ion channel block by acetylcholine, carbachol and suberyldicholine at the frog neuromuscular junction. *Proc. R. Soc. London, Ser. B* 225, 329–355.
30. Mishina, M., Takai, T., Imoto, K., Noda, M., Takahashi, T., Numa, S., Methfessel, C., and Sakmann, B. (1986) Molecular distinction between fetal and adult forms of muscle acetylcholine receptor. *Nature* 321, 406–411.
31. Akk, G., and Auerbach, A. (1996) Inorganic, monovalent cations compete with agonists for the transmitter binding site of nicotinic acetylcholine receptors. *Biophys. J.* 70, 2652–2658.
32. Sanchez, J. A., Dani, J. A., Siemen, D., and Hille, B. (1986) Slow permeation of organic cations in acetylcholine-receptor channels. *J. Gen. Physiol.* 87, 985–1001.
33. Bähring, R., and Mayer, M. L. (1998) An analysis of philanthotoxin block for recombinant rat GluR6(Q) glutamate receptor channels. *J. Physiol.* 509, 635–650.
34. Woodhull, A. M. (1973) Ionic blockade of sodium channels in nerve. *J. Gen. Physiol.* 61, 687–708.
35. de Wolf, I., and van Driessche, W. (1986) Voltage-dependent Ba<sup>2+</sup> block of K<sup>+</sup> channels in apical membrane of frog skin. *Am. J. Physiol.* 251, C696–C706.
36. Dwyer, T. M., Adams, D. J., and Hille, B. (1980) The permeability of the endplate channel to organic cations in frog muscle. *J. Gen. Physiol.* 75, 469–492.
37. Wang, F., and Imoto, K. (1992) Pore size and negative charge as structural determinants of permeability in the *Torpedo* nicotinic acetylcholine receptor channel. *Proc. R. Soc. London, Ser. B* 250, 11–17.
38. Buisson, B., and Bertrand, D. (1998) Open-channel blockers at the human  $\alpha 4 \beta 2$  neuronal nicotinic acetylcholine receptor. *Mol. Pharmacol.* 53, 555–563.
39. Charnet, P., Labarca, C., Cohen, B. N., Davidson, N., Lester, H. A., and Pilar, G. (1992) Pharmacological and kinetic properties of  $\alpha 4 \beta 2$  neuronal nicotinic acetylcholine receptors expressed in *Xenopus* oocytes. *J. Physiol.* 450, 375–394.
40. Papke, R. L., Horenstein, B. A., and Placzek, A. N. (2001) Inhibition of wild-type and mutant neuronal nicotinic acetylcholine receptors by local anesthetics. *Mol. Pharmacol.* 60, 1365–1374.
41. Papke, R. L., Buhr, J. D., Francis, M. M., Choi, K., Thinschmidt, J. S., and Horenstein, N. A. (2005) The effects of subunit composition on the inhibition of nicotinic receptors by the amphipathic blocker 2,2,6,6-tetramethylpiperidin-4-yl heptanoate. *Mol. Pharmacol.* 67, 1977–1990.
42. Gentry, C. L., and Lukas, R. J. (2001) Local anesthetics noncompetitively inhibit function of four distinct nicotinic acetylcholine receptor subtypes. *J. Pharmacol. Exp. Ther.* 299, 1038–1048.

BI800737J